forests

MDPI

Article

Tree Species Classification Based on Sentinel-2 Imagery and Random Forest Classifier in the Eastern Regions of the Qilian Mountains

Minfei Ma [1,2,3], Jianhong Liu [1,2,3,*], Mingxing Liu [1,2,3], Jingchao Zeng [1,2,3] and Yuanhui Li [4]

1 Shaanxi Key Laboratory of Earth Surface System and Environmental Carrying Capacity, Northwest University, Xi'an 710127, China; maminfei@stumail.nwu.edu.cn (M.M.); mingxingliu@stumail.nwu.edu.cn (M.L.); zengjingchao@stumail.nwu.edu.cn (J.Z.)
2 College of Urban and Environmental Science, Northwest University, Xi'an 710127, China
3 Research Institute of the Yellow River in Shaanxi Province, Xi'an 710127, China
4 Northwest Institute of Forest Inventory, Planning and Design, State Forestry Administration, Xi'an 710048, China; nwinventory@sina.com
* Correspondence: jhliu@nwu.edu.cn; Tel.: +86-029-8830-8412

Abstract: Obtaining accurate forest coverage of tree species is an important basis for the rational use and protection of existing forest resources. However, most current studies have mainly focused on broad tree classification, such as coniferous vs. broadleaf tree species, and a refined tree classification with tree species information is urgently needed. Although airborne LiDAR data or unmanned aerial vehicle (UAV) images can be used to acquire tree information even at the single tree level, this method will encounter great difficulties when applied to a large area. Therefore, this study takes the eastern regions of the Qilian Mountains as an example to explore the possibility of tree species classification with satellite-derived images. We used Sentinel-2 images to classify the study area's major vegetation types, particularly four tree species, i.e., *Sabina przewalskii* (S.P.), *Picea crassifolia* (P.C.), *Betula* spp. (Betula), and *Populus* spp. (Populus). In addition to the spectral features, we also considered terrain and texture features in this classification. The results show that adding texture features can significantly increase the separation between tree species. The final classification result of all categories achieved an accuracy of 86.49% and a Kappa coefficient of 0.83. For trees, the classification accuracy was 90.31%, and their producer's accuracy (PA) and user's (UA) were all higher than 84.97%. We found that altitude, slope, and aspect all affected the spatial distribution of these four tree species in our study area. This study confirms the potential of Sentinel-2 images for the fine classification of tree species. Moreover, this can help monitor ecosystem biological diversity and provide references for inventory estimation.

Keywords: Sentinel-2 image; random forest; tree species; vegetation classification

Citation: Ma, M.; Liu, J.; Liu, M.; Zeng, J.; Li, Y. Tree Species Classification Based on Sentinel-2 Imagery and Random Forest Classifier in the Eastern Regions of the Qilian Mountains. *Forests* **2021**, *12*, 1736. https://doi.org/10.3390/f12121736

Academic Editor: Steven L. Petersen

Received: 21 October 2021
Accepted: 7 December 2021
Published: 9 December 2021

1. Introduction

Forests are essential for ecosystem services conservation and ecological protection and work by adjusting local and regional climates, regulating surface heat, modifying watershed-scale hydrological climate, and reducing carbon emissions [1–3]. Forest biodiversity is critical to maintaining forest ecosystems stability. However, it is increasingly threatened by forest fires, forest fragmentation, climate change, and other factors [4]. Trees are the most important components of the forest ecosystem, and tree species information has become one of the critical parameters of interest to ecologists and forest managers [5]. Accurate tree species identification provides a direct means of monitoring forest biodiversity and plays a vital role in ecological change assessment and other forest applications.

Traditional forest ecosystem surveys rely on field surveys to collect tree species information. However, they require heavy human, material, and financial resources and are vulnerable to regional restrictions [6,7]. With the advancement of remote sensing technology, diverse remote sensing data have provided plenty of opportunities for refined tree species identification. For example, Bont et al. [8] used airborne laser scanning data to classify coniferous and broadleaf forests for forest stocks prediction. The study obtained tree canopy heights based on LiDAR data and used them as weights for the wood volume estimation model, which increased the model accuracy by 9%. Mäyrä et al. [9] carried out a classification study to recognize Scots pine, Norway spruce, and Betula and European aspen based on airborne hyperspectral and radar data in Finland's Evo Forest area. They built the normalized canopy height model based on LiDAR data, and realized the recognition and extraction of individual trees. In addition, other remote sensing data have also been widely utilized in tree species classification research, such as point cloud data and unmanned aerial vehicle (UAV) images [10]. The UAV data and LiDAR data work with a high spatial resolution and can extract rich forest canopy texture information and identify single trees. However, the above data are large in volume and difficult to reproduce in the data acquisition environment, so they are suitable for tree species classification experiments in small regions. It is difficult to use such data for regional tree species identification.

Compared with UAV data and airborne laser scanning data, satellite remote sensing data are easier to acquire and process and can be repeatedly observed with a certain period, making them more suitable for regional tree species classification studies. Due to their high spatial resolution (10 m), rich spectral information (13 bands), and short revisit period (2–5 days), Sentinel-2 satellite images have been used in tree species classification experiments [11–13]. However, Sentinel-2 images are challenging to provide satisfactory accuracy in tree species classification when they are not supported by detailed ground survey data [14,15]. In addition to the spectral information, existing studies have found that using topographic metrics and texture features can effectively increase the accuracy of tree species identification in delicate tree species classification based on remote sensing images [16,17]. Different tree species always have distinct growth environments. For example, S.P. is sun-tolerant and grows at an altitude of 2600–4000 m, while P.C. is shade-tolerant and widely distributed within an altitude of 1600–3800 m [18]. The separability of tree species can be enhanced by adding topographic metrics in the classification. Moreover, the texture characteristics computed from the images can reflect the differences in the tree crown structure of different tree species, such as the roughness, size, and shape, and the arrangement of the trees, which can further improve tree species classification. Matheus et al. [16] used WorldView-3 images to classify tropical forest tree species. Their study shows that the classification accuracy increased by over 10% by integrating texture features, compared with only using spectral features.

Due to their excellent performance and clear logic, machine learning algorithms are increasingly used in tree species classifications. Commonly used machine learning algorithms include support vector machine (SVM), Naïve Bayes (NB), Random Forest (RF) classifier, etc. For example, Hu et al. [19] used SVM to classify multiple tree species, including Norway maple and honey locust, with a classification accuracy of 89%. Axelsson et al. [5] classified *Betula* spp., *Picea abies*, *Pinus sylvestris*, and *Quercus robur* based on Bayesian inference and achieved 87% classification accuracy. Xu et al. [10] found that combining multispectral, texture, and point cloud metrics is the best classification scheme based on the three individual tree crown (ITC) delineation algorithm and RF classifier. Compared with other machine learning algorithms, RF classifier is widely used in tree species classification studies because of its good performance in processing high dimensional data and its ability to output the contributions of different features [20]. In recent years, deep learning algorithms have also frequently been used in related studies. Mäyrä et al. [9] compared SVM and three-dimensional convolutional neural networks (3D-CNNs) and found that 3D-CNNs achieved a better performance when classifying LiDAR data. However, there are some shortcomings in the use of deep learning, a considerable drawback and barrier in the use of deep learning is the need for large datasets, and setting data annotation makes the processing of data more complicated [21], which makes the use of deep learning have some limitations.

The Qilian Mountains are located in the northeast arid and semi-arid area of the Qinghai-Tibet Plateau. Due to the impact of global climate change and human activities, the vegetation and biodiversity in the Qilian Mountains are declining, and the function of soil and water conservation continues to weaken [22]. These problems have seriously affected the stability of the Qilian Mountain ecosystems and restricted the social and economic sustainable development of its surrounding areas. Therefore, understanding the spatial distribution of different tree species in this area is a key issue. This research takes the eastern regions of the Qilian Mountains as an example to investigate the possibility of using Sentinel-2 imagery and the random forest classifier for delicate tree species classification, as well as to depict the spatial distribution characteristics of its main tree species, and aims to provide guidance for local forest management and ecological assessment.

2. Study Area and Data

2.1. Study Area

The study area is located in the northeastern part of Qinghai Province, China. Considering the ground samples are mainly located in the eastern part of Qilian, the study area is defined as the eastern Qilian Mountains (Figure 1). Its geographical extent is 101°10′ E~102°53′ E, 35°48′ N~37°25′ N. The total area is 18,182 km^2. This area has high altitudes and a frigid climate. The altitude ranges from 1674 m to 4720 m, with a relative elevation difference of 3015 m. The climate in the study area is a typical alpine continental climate, with an average annual temperature of 2.1 °C, annual precipitation of 366 mm, an altitude of 1674 m–4720 m, and a relative elevation difference of 3015 m. As the temperature and precipitation change with altitudes, local vegetation distribution presents an apparent vertical zonality. From low to high altitudes, this region can be divided into a mountain steppe zone, temperate shrub-steppe zone, mountain forest-steppe zone, subalpine shrub-meadow zone, and alpine sub-icy, and sparse vegetation zone [23]. The existing main tree species are *Sabina przewalskii*, *Picea crassifolia*, *Betula* spp., and *Populus* spp. [24].

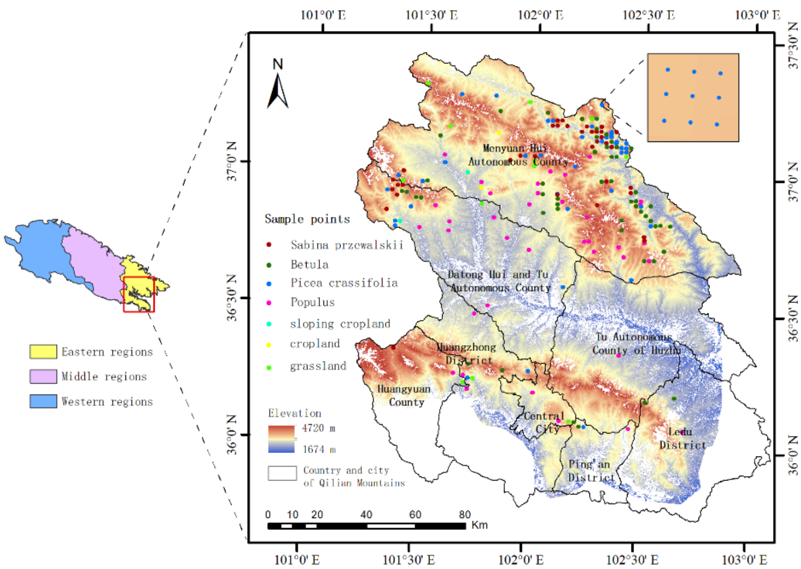

Figure 1. The geographical location of the study area and an illustration of nine samples in a sample plot.

It is also one of the critical water conservation areas along the Hexi Corridor and one of the vital water supply areas for the Yellow River and Qinghai Lake. The Qilian Mountains have an important strategic position in constructing China's ecological civilization and have formed a unique ecological barrier in the northwest region [25]. As it is in the transition zone from a temperate continental climate to a plateau mountain climate, the special geographical location and climate type determine the fragile ecological environment of the Qilian Mountains [22,24]. Therefore, accurate and refined vegetation information is essential for protecting the ecological environment of the Qilian Mountains.

2.2. Data Source and Preprocessing

Three data types are used in this research to accurately identify different vegetation types in the study area, namely, Sentinel-2 images, Digital Elevation Model (DEM) data, and field data. Sentinel-2 provides images with satisfactory spatial resolution, revisit cycle, and abundant spectral bands among all free-accessed satellite data [26,27]. It has been widely used in many fields, such as vegetation type identification, forest resource monitoring, food safety assurance, and environmental monitoring. In particular, the three red-edge bands and two near-infrared bands designed by Sentinel-2 provide a possible solution for identifying forest tree species. The spectral parameters used in the research are shown in Table 1. In total, eight scenes of Sentinel-2 imagery (L1C level) cover with the study area with less cloud cover in 2020 were acquired from the Copernicus Open Access Center [28]. Six images were acquired on 20 August, and the other two were on 25 August and 4 September, respectively. All of the images were atmospherically and topographically corrected with the Sen2Cor plug-in provided by the European Space Agency [29]. Then, image bands with a resolution of 20 m were resampled to 10 m by using the Sentinel Application Platform (SNAP). After that, all 10 m Sentinel-2 bands of each scene were layer-stacked to produce a ready-to-use image.

Table 1. The parameters of the Sentinel-2 spectral bands used in this study.

Spectral Bands	Central Wavelength (nm)	Bandwidth (nm)	Spatial Resolution (m)
Blue	490	98	10
Green	560	45	10
Red	665	38	10
Vegetation Red Edge 1	705	19	20
Vegetation Red Edge 2	740	18	20
Vegetation Red Edge 3	775	28	20
Near InfraRed	842	145	10
Narrow Near InfraRed	865	33	20
Short Wave InfraRed	1610	143	20
Short Wave InfraRed	2190	242	20

As topography significantly affects the distribution of forest tree species in mountain ecosystems, considering the topographic metrics in classification can effectively improve classification accuracy [17]. Therefore, we downloaded the Advanced Land Observing Satellite digital elevation model (ALOS DEM) data from the National Aeronautics and Space Administration [30]. The data have a spatial resolution of 12.5 m, which contains richer terrain details than the 30 m DEM. Then, we calculated the slope and aspect based on the DEM data. Finally, the DEM data, slope data, and aspect data were resampled to 10 m.

The ground samples were provided by the Northwest Survey, Planning, and Design Institute of National Forestry and Grassland Administration of China. The ground samples were collected through the Qinghai Provincial Forest Resources Survey in 2018. There were a total of 149 ground sample plots within the study area, and each sample plot recorded information about tree species, breast-height diameter, canopy closure, average height, etc. As one survey sample plot is a rectangle that covers 800 m^2, it is close to the coverage area of 3 $\times$ 3 Sentinel-2 pixels (900 m^2). Therefore, nine pixels covered by the sample plot are all collected as candidate samples for the same tree species. Then, we verified the reliability of these extended samples based on the Google Earth image in 2020, and deleted the unqualified samples. Through this method, we obtained samples for S.P., P.C., Betula, and Populus. In addition, we also visually interpreted samples of other vegetation types (cropland, sloping cropland, and grasslands) in the study area based on the Google Earth images in 2020. Finally, 1721 samples were obtained for classification (Figure 1), of which 2/3 were used as training samples, and the rest were used as test samples to verify the classification accuracy.

3. Methods

3.1. Calculation of Vegetation Indices

Many studies in vegetation classification have proved that vegetation indices can effectively enhance the spectral information of remote sensing data [31,32]. The rich spectral bands of Sentinel-2 images facilitate calculating various vegetation indices. In this study, we calculated four vegetation indices, the Normalized Difference Vegetation Index (*NDVI*), the Red Edge Normalized Difference Vegetation Index ($NDVI_{705}$), the Enhanced Vegetation Index (*EVI*), and the Land Surface Water Index (*LSWI*). Among them, *NDVI* is the best indicator reflecting the growth status of vegetation [33,34], and $NDVI_{705}$ is a normalized vegetation index based on the red edge band. Compared with *NDVI*, $NDVI_{705}$ is more sensitive to small changes in the leaf canopy [35]. *EVI* reacts more strongly to vegetation growth in lush areas and can effectively reduce the impact of water vapor [34]. *LSWI* is more sensitive to leaf moisture and can eliminate water interference while identifying vegetation [36]. Therefore, we calculated the above four vegetation indices to improve the identification ability of the mountain tree species in the eastern region of the Qilian Mountains. The calculation formulas are shown as follows:

$$NDVI = \frac{B_{nir} - B_{red}}{B_{nir} + B_{red}} \tag{1}$$

$$NDVI_{705} = \frac{B_{705} - B_{red}}{B_{705} + B_{red}} \tag{2}$$

$$EVI = 2.5 \times \frac{B_{nir} - B_{red}}{B_{nir} + 6 \times B_{red} - 7.5 \times B_{blue} + 1} \tag{3}$$

$$LSWI = \frac{B_{nir} - B_{swir}}{B_{nir} + B_{swir}} \tag{4}$$

B_{blue} is the blue band, B_{red} is the red band, B_{705} is the red edge band with a centre wavelength of 0.705 nm, B_{nir} is the near-infrared band, and B_{swir} is the shortwave infrared band, corresponding to the B2, B4, B5, B8, and B11 bands of the Sentinel-2 image, respectively (Table 1).

3.2. Extraction of Texture Features

The grey level co-occurrence matrix (GLCM) is commonly used in remote sensing image classification to analyze and extract texture features. GLCM counts the grey levels of different pixels on the image [37,38] and gets a series of statistics. Haralick has proposed 14 statistics based on the grey level co-occurrence matrix [38], such as contrast, entropy, correlation, uniformity, and variance. Among them, contrast reflects the clarity and texture characteristics of the image. The entropy value represents the complexity of the image grey distribution. The larger the entropy value, the more complex the image. The correlation reflects the similarity of the image grey level in the row or column direction. The size reflects the correlation of the local image. The larger the value, the more significant the correlation.

Before obtaining GLCM statistics, we need to perform principal component analysis (PCA) first to derive the first principal component (PC_1). PC_1 explains 90.52% of the variance, which means most of the information concentrated in PC1 [39]. Then, we calculated the mean, variance, homogeneity, contrast, dissimilarity, entropy, second moment, and correlation based on PC_1.

3.3. Extraction of Vegetated Area

As this research aims to classify different vegetation types, it is better to mask out the non-vegetated areas [5]. *NDVI* is the most widely used vegetation index, and determining an appropriate *NDVI* threshold to classify non-vegetation and vegetation requires many tests for different study areas. Therefore, we conducted a threshold test by setting *NDVI* threshold changes from 0.18 to 0.40 with an increasement of 0.02 every time. The masked results were visually interpreted based on Google Earth images. When the *NDVI* threshold is smaller than 0.30, there are still many non-vegetated areas, and when the threshold is greater than 0.30, over-masking will occur (Figure 2). We find that when the *NDVI* threshold is set as 0.30, the derived vegetated area is mostly in agreement with the Google Earth images. Therefore, the non-vegetated area of the entire study area is masked based on the optimal *NDVI* threshold of 0.3. Finally, the vegetation area in the study area is 14,364 km^2, accounting for 79% of the study area.

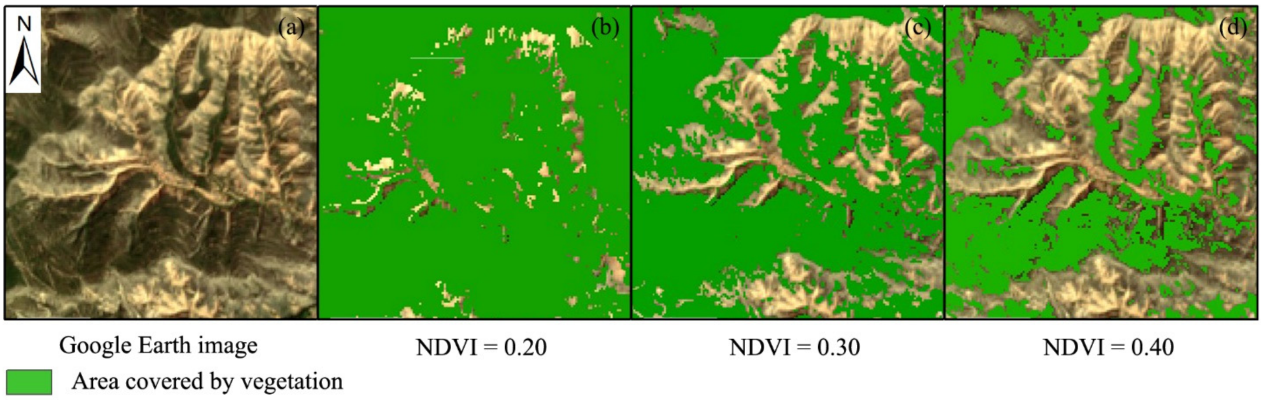

Figure 2. Comparison of vegetated area extracted with different *NDVI* thresholds based on Google Earth images. (**a**) Original Google Earth image, (**b**–**d**) are masks with thresholds of 0.2, 0.3, and 0.4, respectively.

3.4. Random Forest Classifier

The RF classifier contains multiple decision trees, and the classification result is determined by the majority voting of all of the trees [20]. This integrated classifier will have better accuracy in data regression and classification problems, while making the algorithm more stable and robust [40]. In addition, RF can handle the multi-dimensional data used in tree species identification, and is not prone to overfitting. Compared with the maximum likelihood classification (MLC) algorithms [41], the random forest algorithm has a better performance in the analysis of the high dimensional data. Meanwhile, as an object-oriented classification method, RF is more tolerant and flexible for input features than the SVM algorithm [42]. The RF classifier achieves better performance in many applications, and is widely used in economic [43,44] and social [45] studies and in other research fields. Moreover, this classifier is very popular within the remote sensing community, such as forestry [17], agriculture [46], and land resources [47] departments.

Therefore, we chose the random forest classifier to classify the tree species in the eastern regions of the Qilian Mountains. We designed three classification schemes to analyze the effects of spectral features, topographic metrics, and texture features on the separability of different tree species and chose the best separability scheme for tree species classification:

(1) Scheme 1: Use only spectral features (10 spectral bands plus four vegetation indices, totally 14 features).

(2) Scheme 2: Spectral features + topographic metrics (17 features).

(3) Scheme 3: Spectral features + topographic metrics + texture features (25 features).

The RF classifier in the research was based on the "randomForest" plug-in in ENVI 5.3. After repeated testing, the parameter ntree (number of trees) was set to be 800, and the feature digit (mtry) used on each node iwas the square root of the total number of input features [20,48].

To assess the accuracy of the tree species classification using Sentinel-2 images, we calculated the overall accuracy (OA), Kappa coefficient, producer's accuracy (PA), and user's accuracy (UA) based on the ground testing samples confusion matrix [49].

4. Results

4.1. Separability Analysis of Different Schemes

In order to illustrate the separability of different vegetation types under different classification schemes, we calculated the pairwise separability between the various classes based on Jeffries–Matusita (JM) distance [50]. JM distance value ranges from 0 to 2, and a higher JM value indicates stronger separability of two classes. In this study, the JM distance is divided into four levels: strong separation (1.9–2.0), good separation (1.8–1.9), weak separation (1.7–1.8), and poor separation (<1.7). A JM distance between each two different classes greater than 1.8 is required for a satisfactory classification. Figure 3a–c represents the separability under the three classification schemes, respectively. Under Scheme 1, trees and non-trees can be well separated. However, the distinction between closer vegetation classes is poor, such as P.C. vs. Populus and cropland vs. sloping cropland.

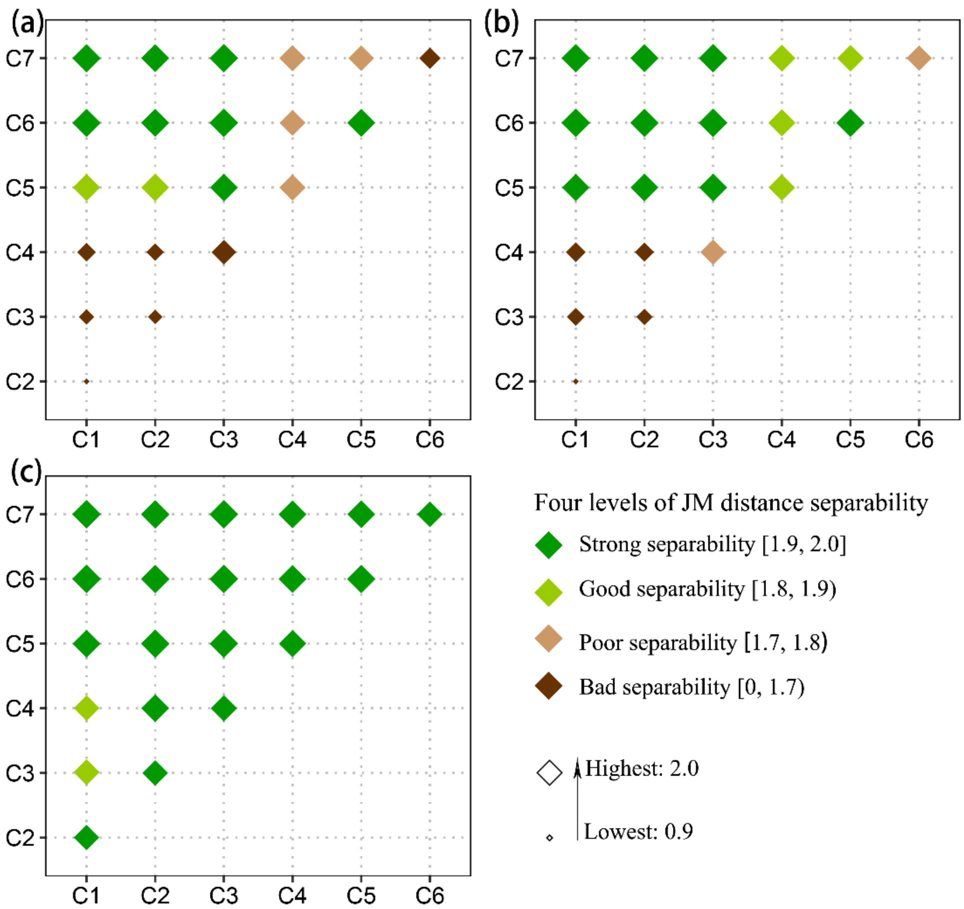

Figure 3. Class separability under (**a**) Scheme 1, (**b**) Scheme 2 and (**c**) Scheme 3 based on JM distance, C1 to C7 represent *Sabina przewalskii*, Betula, *Picea crassifolia*, Populus, grassland, cropland and sloping cropland, respectively.

Under Scheme 2, the overall separability has significantly increased. The separability of cropland, sloping cropland, and grassland increased, but it is still difficult to classify. Figure 3c shows all JM distances are greater than 1.9, except for S.P. vs. P.C. and S.P. vs. Populus, which means combining topographic metrics and texture features can effectively increase the separation between similar vegetation categories. In particular, the texture features can well classify different tree species, such as Betula and P.C., P.C. and Populus, and cropland and sloping cropland. This strongly shows that the texture features of Sentinel-2 images can enhance the separability of tree species.

4.2. Classification Accuracy

Considering the separability of different types in the three schemes, the final classification result is based on Scheme 3. The accuracy assessment results show that the overall accuracy is 86.49%, with the Kappa coefficient of 0.83 (Figure 4a). Compared with non-trees, the trees showed a better recognition potential with higher PA and UA, indicating a satisfying performance of Sentinel-2 in recognition of tree species. However, the results also demonstrate that the classification of non-trees was relatively poor, especially in sloping cropland with a UA of 54.17%. The complex distribution of farmland, roads, and water systems in the study area resulted in many misclassifications of vegetation types, especially in river valleys and flat regions.

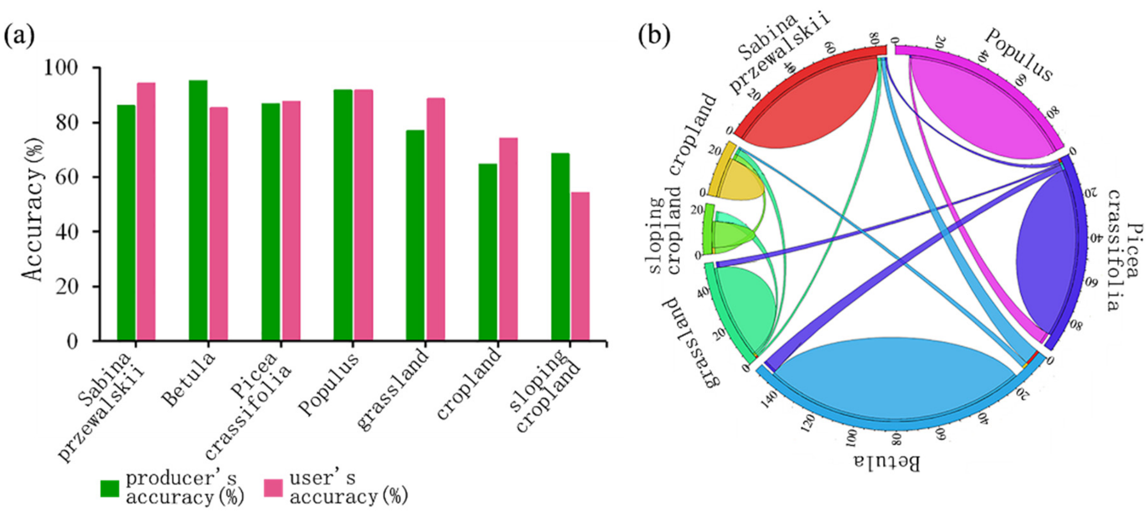

Figure 4. Classification accuracies of Scheme 3. (**a**) PAs and UAs of different vegetation types, (**b**) misclassifications between different vegetation types.

Based on the chord diagram, more detailed misclassifications between different vegetation types are analyzed (Figure 4b). Each arc represents the correctly classified samples of one vegetation class, and the links between different classes represent misclassifications. The width of each link indicates the number of misclassified samples. The wider the link, the more the misclassified samples. Taking Betula as an example, the purple link on the left indicates the wrong classification of other classes into Betula, while the blue link on the right means the misclassification of Betula into other classes. There are few misclassifications between the four trees, while the non-trees are more seriously misclassified, such as grassland vs. farmland and grassland vs. sloping farmland. Because of the growth of weeds in the field, there is an apparent spectral similarity between cropland, grassland and sloping cropland, making it difficult to classify non-trees.

4.3. Spatial Distribution Patterns of Different Vegetation Types

The spatial distribution of different vegetation types is presented in Figure 5. It shows that trees mostly grow at mid-altitude or high-altitude areas, covering 8286 km^2, and accounting for 57.7% of the vegetated area of this region. Cropland and sloping cropland are located near residential places, with a gentle slope, suitable temperature and precipitation, which favors production. Grassland is the buffer zone between trees and cultivated land, with an area of 2740 km^2.

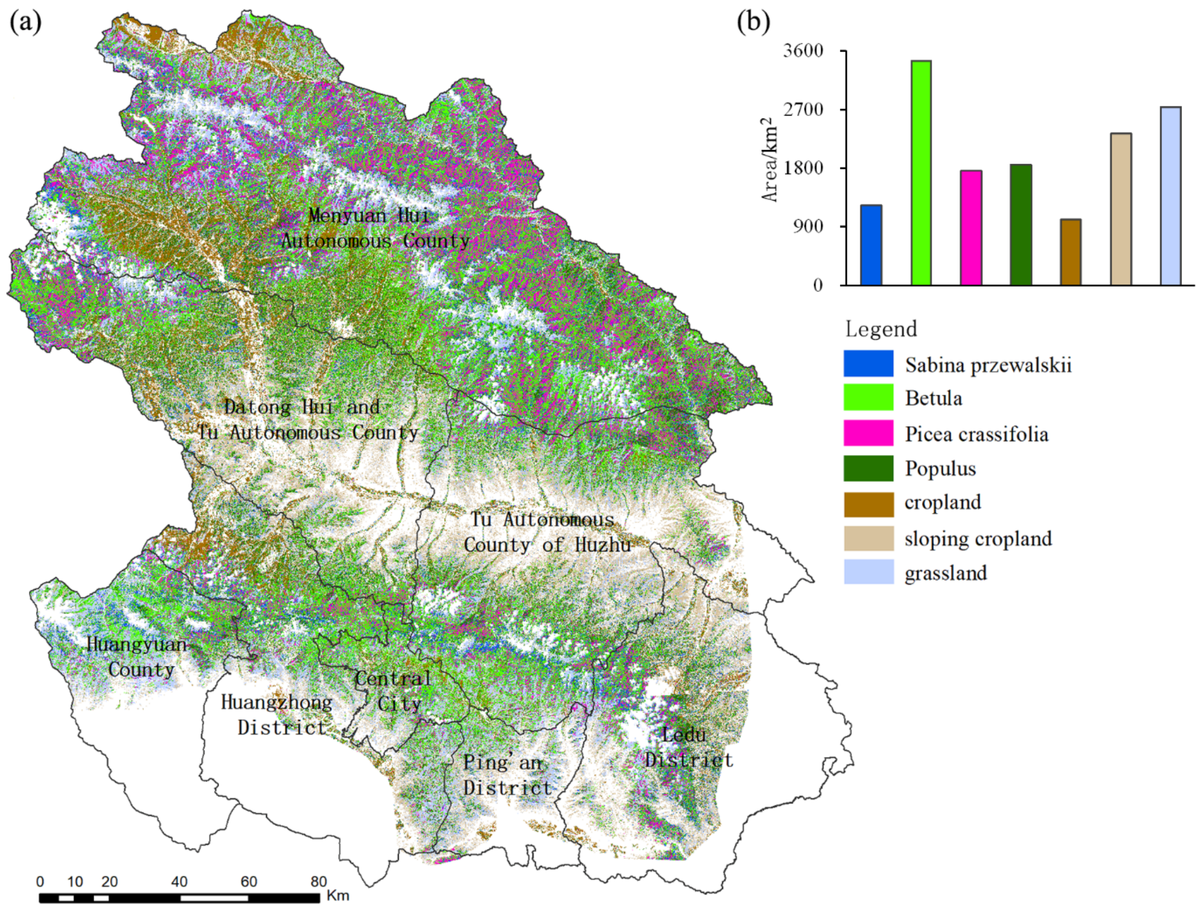

Figure 5. The spatial distribution patterns (**a**) and acreages (**b**) of different vegetation types.

The area of Betula is 3447.6 km^2, accounting for 41.6% of the total, which is the dominant tree species among the four tree species. The acreages of P.C. and Populus are 1575.6 km^2 and 1851.7 km^2, respectively. The area of S.P. is 1229.2 km^2, which is the least. The Betula is mainly *Betula platyphylla* in the study area, an important temperate forest component. As a pioneer tree species in the forest, *Betula platyphylla* indicates that the forest is in the transitional stage of community succession. The large area of Betula represents that the forest ecosystem of the Qilian Mountains is unstable and fragile.

4.4. Geographical Distribution Characteristics of Different Tree Species

The separability schemes show that adding topographic metrics can increase the separability between different tree species. Moreover, the classification result presents a prominent distribution characteristic of "Populus−Betula−P.C.−S.P.", extending from the river valley to the ridge. Therefore, we try to explore the relationship between topographic metrics and tree species distribution in altitude and slope. We count the area of trees with a 500 m interval, and Figure 6a shows that the four tree species mainly grow in the range of 2500–3500 m. In general, the acreage of the four tree species increases first and then decreases with attitude. Populus tend to grow between 2500 and 3000 m, and also above 4000 m. The growing regions of Betula and P.C. are similar, mainly distributed in 2500–3500 m, but Betula mainly grows at an altitude above 4000 m. S.P. is mostly distributed within altitudes between 2000 and 3500 m, and its area increases as the altitude increases.

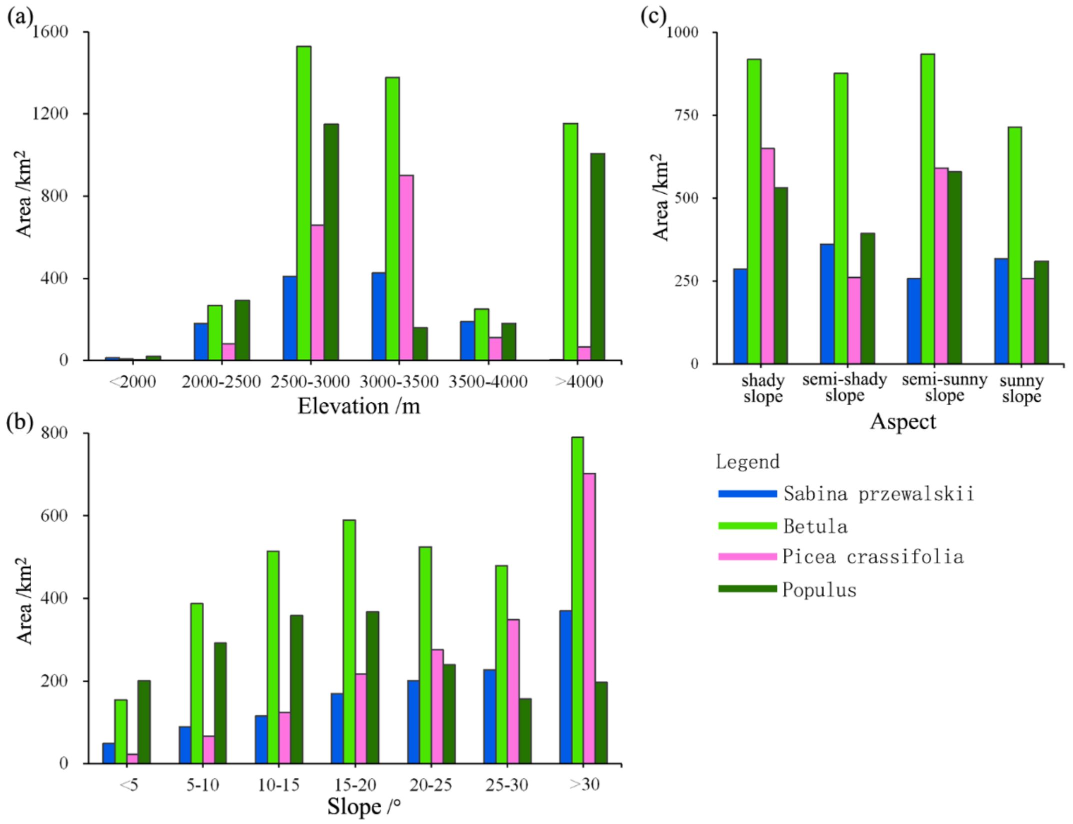

Figure 6. Spatial distribution of the four arbor tree species on (**a**) altitude, (**b**) slope, and (**c**) aspect.

Concerning the slope, the area of trees is counted at every 5° interval, and the result is shown in Figure 6b. The area of S.P. and P.C. keep increasing with the slope, and the acreage of Betula and Populus increase first and then decrease between 5° and 30°. The four tree species have specific tendencies to sunlight. Therefore, we analyzed the distribution of tree species on the different aspects (Figure 6c). This shows that P.C. and Populus mostly grow on shady and semi-sunny slopes, while S.P. and Betula are evenly distributed in every aspect.

Although the distribution of different tree species in altitude, slope, and aspect overlaps, combining three topographic metrics can effectively increase the separability of tree species, which is consistent with some previous studies [17,46,51].

5. Discussion

Remote sensing-assisted tree species classification is driven by various forest management and ecological protection departments [31,52]. In the past 40 years, studies on tree species classification have been increasing, especially based on airborne multispectral sensors [8,9]. However, many researches focus on identifying broad tree species, such as coniferous and broadleaf forests, and there is less researches regarding more detailed tree species classification, especially using satellite images. Therefore, this research explored the possibility of using Sentinel-2 multispectral images to classify four arbor tree species (S.P., Betula, P.C., and Populus) in the eastern region of the Qilian Mountains in China.

Although this study confirms the great potential of Sentinel-2 images in the refined tree species classification, there are still two limitations. First, although vegetation indices and texture features are the primary basis for identifying tree species, ground tree species information is equally important. The relatively high accuracy of tree species classification in this study is possibly resulted from the way we collected tree species samples. The tree species samples used in this article are mainly derived from the ground survey samples of the Qinghai Province Forest Resources Survey in 2018, accounting for 78% of all of the sample data. Each ground survey sample generated nearly nine classification samples, and these nine samples are concentrated in the same space, and their spectral characteristics and topographic metrics are highly similar. Due to the limitation of experimental conditions, we can not collect an ideal sample set. Alternatively, UAV images and airborne laser scanning data can provide training samples with a more reasonable spatial distribution, which will improve the collection of training and validation samples and eventually promote tree species classification with satellite images [53,54].

Second, texture feature is important in differentiating tree species. However, the texture information is calculated from Sentinel-2 images with a 10 m spatial resolution in this study, which is insufficient. Remote sensing images with a sufficiently high spatial resolution can provide rich texture information, and texture details such as canopy shape, size, and roughness, can help in accurate tree species identification. Thus, a possible way to acquire more detailed texture information is to integrate high-resolution satellite imagery, such as GaoFen-2 Pan-Multispectral (GF-2 PMS) images, in classification. Moreover, the feature geometry and surface features provided by spaceborne LiDAR can compensate for the deficiencies of optical remote sensing images [48,53]. Nowadays, spaceborne LiDAR data are proliferating [54], and it is easier to obtain data at any time and area. Assimilating information from both optical images and LiDAR data in tree species classification may be another way to boost tree species classification. Therefore, remote sensing images with a high spatial resolution and LiDAR data for the accurate classification of tree species is a practical and feasible approach.

6. Conclusions

Accurate tree species information is essential for ecological assessment and other forest applications, especially for the ecologically fragile Qilian Mountains. Therefore, based on the Sentinel-2 image with a spatial resolution of 10 m and the random forest algorithm, our research achieved high-precision and refined recognition of the existing main tree species (S.P., Birch, P.C., and Populus) in the eastern region of the Qilian Mountains.

(1) The overall accuracy of tree species classification is 86.49%, and the Kappa coefficient is 0.83. Compared with non-tree forests (grassland, cropland, and sloping cropland), the recognition of the trees is better, and their PA and UA are higher than 84.97%. However, there are certain misclassifications and omissions, especially between grassland and cropland, grassland, and sloping cropland.

(2) Altitude, slope and aspect all affect the spatial distribution of the tree species. Except for Populus, other tree species generally show a "first increase-then decrease" trend as the altitude increases. At the same time, various tree species also show significant differences in slope and aspect. Although the distribution of different tree species in altitude, slope, and aspect overlaps, combining the three topographic metrics can distinguish different tree species.

(3) After comparing separability, adding texture features makes the separability between vegetation categories greater than 1.9, and the separability is good. Only the separability between S.P. and P.C., S.P., and Populus is greater than 1.8, and the separation is qualified. Texture features effectively increase the separability of tree species.

In general, Sentinel-2 images have great potential in the delicate monitoring and identification of tree species. Classification and monitoring of tree species in ecologically fragile areas can assist in regional ecological assessment and forest protection and provide meaningful guidance for realizing automatic forest inventory and government decision-making.

Author Contributions: Data curation, M.M., M.L., J.Z. and Y.L.; Formal analysis, M.M. and J.L.; Funding acquisition, J.L.; Methodology, M.M. and J.L.; Supervision, J.L.; Writing—original draft, M.M. and J.L. All authors have read and agreed to the published version of the manuscript.

Funding: This research was funded by China's National Natural Science Foundation (NO. 41401494) and the Natural Science Foundation of Shaanxi Provincial Department of Education (NO. 14JK1745).

Institutional Review Board Statement: Not applicable.

Informed Consent Statement: Not applicable.

Data Availability Statement: Not applicable.

Conflicts of Interest: The authors declare no conflict of interest.

References

1. Shafizadeh-Moghadam, H.; Minaei, M.; Feng, Y.; Pontius, R.G. GlobeLand30 maps show four times larger gross than net land change from 2000 to 2010 in Asia. *IJAEO Int. J. Appl. Earth Obs. Geoinf.* **2019**, *78*, 240–248. [CrossRef]
2. Pulitia, S.; Breidenbacha, J.; Schumachera, J.; Hauglina, M.; Klingenbergb, T.F.; Astrupa, R. Above-ground biomass change estimation using national forest inventory data with Sentinel-2 and Landsat. *Remote Sens. Environ.* **2021**, *265*, 112644. [CrossRef]
3. Parhizkar, M.; Shabanpour, M.; Miralles, I.; Zema, D.A.; Lucas-Borja, M.E. Effects of plant species on soil quality in natural and planted areas of a forest park in northern Iran. *Sci. Total Environ.* **2021**, *778*, 146310. [CrossRef]
4. Durães, R.; Carrasco, L.; Smith, T.B.; Karubian, J. Effects of forest disturbance and habitat loss on avian communities in a Neotropical biodiversity hotspot. *Biol. Conserv.* **2013**, *166*, 203–211. [CrossRef]
5. Axelsson, A.; Lindberg, E.; Reese, H.; Olsson, H. Tree species classification using Sentinel-2 imagery and Bayesian inference. *IJAEO Int. J. Appl. Earth Obs. Geoinf.* **2021**, *100*, 102318. [CrossRef]
6. Persson, M.; Lindberg, E.; Reese, H. Tree Species Classification with Multi-Temporal Sentinel-2 Data. *Remote Sens.* **2018**, *10*, 1794. [CrossRef]
7. Fassnacht, F.E.; Latifi, H.; Stereńczak, K.; Modzelewska, A.; Lefsky, M.; Waser, L.T.; Straub, C.; Ghosh, A. Review of studies on tree species classification from remotely sensed data. *Remote Sens. Environ.* **2016**, *186*, 64–87. [CrossRef]
8. Bont, L.G.; Hill, A.; Waser, L.T.; Bürgi, A.; Ginzler, C.; Blattert, C. Airborne-laser-scanning-derived auxiliary information discriminating between broadleaf and conifer trees improves the accuracy of models for predicting timber volume in mixed and heterogeneously structured forests. *For. Ecol. Manag.* **2020**, *459*, 117856. [CrossRef]
9. Mäyrä, J.; Keski-Saari, S.; Kivinen, S.; Tanhuanpää, T.; Hurskainen, P.; Kullberg, P.; Poikolainen, L.; Viinikka, A.; Tuominen, S.; Kumpula, T.; et al. Tree species classification from airborne hyperspectral and LiDAR data using 3D convolutional neural networks. *Remote Sens. Environ.* **2021**, *256*, 112322. [CrossRef]
10. Xu, Z.; Shen, X.; Cao, L.; Coops, N.C.; Goodbody, T.R.H.; Zhong, T.; Zhao, W.; Sun, Q.; Ba, S.; Zhang, Z.; et al. Tree species classification using UAS-based digital aerial photogrammetry point clouds and multispectral imageries in subtropical natural forests. *IJAEO Int. J. Appl. Earth Obs. Geoinf.* **2020**, *92*, 102173. [CrossRef]
11. Immitzer, M.; Atzberger, C.; Koukal, T. Tree Species Classification with Random Forest Using Very High Spatial Resolution 8-Band WorldView-2 Satellite Data. *Remote Sens.* **2012**, *4*, 2661–2693. [CrossRef]
12. Bolyn, C.; Michez, A.; Gaucher, P.; Lejeune, P.; Bonnet, S. Forest mapping and species composition using supervised per pixel classification of Sentinel-2 imagery. *Biotechnol. Agron. Soc. Environ.* **2018**, *22*, 172–187.
13. Soleimannejad, L.; Ullah, S.; Abedi, R.; Dees, M.; Koch, B. Evaluating the potential of sentinel-2, landsat-8, and irs satellite images in tree species classification of hyrcanian forest of iran using random forest. *J. Sustain. For.* **2019**, *38*, 615–628. [CrossRef]
14. Li, W.; Niu, Z.; Shang, R.; Qin, Y.; Wang, L.; Chen, H. High-resolution mapping of forest canopy height using machine learning by coupling ICESat-2 LiDAR with Sentinel-1, Sentinel-2 and Landsat-8 data. *IJAEO Int. J. Appl. Earth Obs. Geoinf.* **2020**, *92*, 102163. [CrossRef]
15. Caballero, I.; Stumpf, R.P. On the use of Sentinel-2 satellites and lidar surveys for the change detection of shallow bathymetry: The case study of North Carolina inlets. *Coast. Eng.* **2021**, *169*, 103936. [CrossRef]
16. Ferreira, M.P.; Wagner, F.H.; Aragão, L.E.O.C.; Shimabukuro, Y.E.; de Souza Filho, C.R. Tree species classification in tropical forests using visible to shortwave infrared WorldView-3 images and texture analysis. *ISPRS J. Photogram. Remote Sens* **2019**, *149*, 119–131. [CrossRef]
17. Liu, M.; Liu, J.; Atzberger, C.; Jiang, Y.; Ma, M.; Wang, X. Zanthoxylum bungeanum Maxim mapping with multi-temporal Sentinel-2 images: The importance of different features and consistency of results. *ISPRS J. Photogram. Remote Sens.* **2021**, *174*, 68–86. [CrossRef]
18. Song, W.; Mu, C.; Zhang, Y.; Zhang, X.; Li, Z.; Zhao, H.; Wang, X. Moisture-driven changes in the sensitivity of the radial growth of Picea crassifolia to temperature, northeastern Tibetan Plateau. *Dendrochronologia* **2020**, *64*, 125761. [CrossRef]
19. Hu, B.; Li, Q.; Hall, G.B. A decision-level fusion approach to tree species classification from multi-source remotely sensed data. *ISPRS Open J. Photogramm. Remote. Sens.* **2021**, *1*, 100002. [CrossRef]
20. Belgiu, M.; Drăguţ, L. Random forest in remote sensing: A review of applications and future directions. *ISPRS J. Photogram. Remote Sens.* **2016**, *114*, 24–31. [CrossRef]
21. Kamilaris, A.; Prenafeta-Boldú, F.X. Deep learning in agriculture: A survey. *Comput. Electron. Agric.* **2018**, *147*, 70–90. [CrossRef]
22. Zongxing, L.; Qi, F.; Zongjie, L.; Xufeng, W.; Juan, G.; Baijuan, Z.; Yuchen, L.; Xiaohong, D.; Jian, X.; Wende, G.; et al. Reversing conflict between humans and the environment—The experience in the Qilian Mountains. *Renew. Sustain. Energy Rev.* **2021**, *148*, 111333. [CrossRef]

23. Fu, X.J.; Cao, G.C.; Guo, W.J. Changes of growing season NDVI at differet elevations, slopes, slope aspect and its relationship with meteorological factors in the southern slope of the Qilian Mountains, China from 1998 to 2017. *Chin. J. Appl. Ecol.* **2020**, *31*, 1203–1212.
24. Li, M. Classification of Picea Crassifolia and Sabina Przewalskii Based on Multi-Source Remote Sensing Images—A Case Study of Qilian Mountain National Park. Master's Thesis, Lanzhou University, Lanzhou, China, 2020.
25. Tang, Z.H.; Yu, Q.S.; Liu, H.J.; Jiang, S.X. Characteristics of alpine vegetation community and its relationship to topographic climate factors in the eastern Qilian mountain. *Acta Ecol. Sin.* **2020**, *40*, 223–232.
26. Bhattarai, R.; Rahimzadeh-Bajgiran, P.; Weiskittel, A.; Meneghini, A.; MacLean, D.A. Spruce budworm tree host species distribution and abundance mapping using multi-temporal Sentinel-1 and Sentinel-2 satellite imagery. *ISPRS J. Photogram. Remote Sens* **2021**, *172*, 28–40. [CrossRef]
27. Ruiz, L.F.C.; Guasselli, L.A.; Simioni, J.P.D.; Belloli, T.F.; Barros Fernandes, P.C. Object-based classification of vegetation species in a subtropical wetland using Sentinel-1 and Sentinel-2A images. *Sci. Remote Sens.* **2021**, *3*, 100017. [CrossRef]
28. Copernicus Open Access Center. Available online: https://scihub.copernicus.eu/dhus/#/home (accessed on 7 April 2021).
29. European Space Agency. Available online: https://www.esa.int/ (accessed on 7 April 2021).
30. National Aeronautics and Space Administration. Available online: https://search.asf.alaska.edu/#/ (accessed on 10 April 2021).
31. Liu, W.; Dong, J.; Xiang, K.; Wang, S.; Han, W.; Yuan, W. A sub-pixel method for estimating planting fraction of paddy rice in Northeast China. *Remote Sens. Environ.* **2017**, *205*, 305–314. [CrossRef]
32. Shin, J.-I.; Seo, W.-W.; Kim, T.; Park, J.; Woo, C.-S. Using UAV Multispectral Images for Classification of Forest Burn Severity—A Case Study of the 2019 Gangneung Forest Fire. *Forests* **2019**, *10*, 1025. [CrossRef]
33. Norris, J.R.; Walker, J.J. Solar and sensor geometry, not vegetation response, drive satellite NDVI phenology in widespread ecosystems of the western United States. *Remote Sens. Environ.* **2020**, *249*, 112013. [CrossRef]
34. Shammi, S.A.; Meng, Q. Use time series NDVI and EVI to develop dynamic crop growth metrics for yield modeling. *Ecol. Indic.* **2021**, *121*, 107124. [CrossRef]
35. Adeyeri, O.E.; Akinsanola, A.A.; Ishola, K.A. Investigating surface urban heat island characteristics over Abuja, Nigeria: Relationship between land surface temperature and multiple vegetation indices. *Remote Sens. Appl. Soc. Environ.* **2017**, *7*, 57–68. [CrossRef]
36. Zhang, Y.S.; Xie, Y.L. Vegetation Water Content Estimation Using NDVI and LSWI from MODIS Images. *Sci. Geogr. Sin.* **2008**, *28*, 72–76.
37. Harlick, R.M.; Shanmugam, K. Textural Features for Image Classification. *IEEE Trans. Syst. Man Cybern.* **1973**, *SMC-3*, 610–621.
38. Hawlick, R.M. Statistical and Structural Approaches to Texture. *Proc. IEEE* **1979**, *67*, 786–804.
39. Dabiri, Z.; Lang, S. Comparison of Independent Component Analysis, Principal Component Analysis, and Minimum Noise Fraction Transformation for Tree Species Classification Using APEX Hyperspectral Imagery. *ISPRS Int. J. Geo-Inf.* **2018**, *7*, 488. [CrossRef]
40. Qiao, Y.; Chen, H.; Jiang, Y. Quantifying the impacts of lithology on vegetation restoration using a random forest model in a karst trough valley, China. *Ecol. Eng.* **2020**, *156*, 105973. [CrossRef]
41. Chutia, D.; Bhattacharyya, D.K.; Sarma, K.K.; Kalita, R.; Sudhakar, S. Hyperspectral Remote Sensing Classifications: A Perspective Survey. *Trans. GIS* **2016**, *20*, 463–490. [CrossRef]
42. Ghosh, A.; Joshi, P.K. A comparison of selected classification algorithms for mapping bamboo patches in lower Gangetic plains using very high resolution WorldView 2 imagery. *IJAEO Int. J. Appl. Earth Obs. Geoinf.* **2014**, *26*, 298–311. [CrossRef]
43. Kaczmarczyk, K.; Hernes, M. Financial decisions support using the supervised learning method based on random forests. *Procedia Comput. Sci.* **2020**, *176*, 2802–2811. [CrossRef]
44. Makariou, D.; Barrieu, P.; Chen, Y. A random forest based approach for predicting spreads in the primary catastrophe bond market. *Insur. Math. Econ.* **2021**, *101*, 140–162. [CrossRef]
45. Haraa, H.; Fujita, Y.; Tsuda, K. Population estimation by random forest analysis using Social Sensors. *Procedia Comput. Sci.* **2020**, *176*, 1893–1902. [CrossRef]
46. Li, R.; Xu, M.; Chen, Z.; Gao, B.; Cai, J.; Shen, F.; He, X.; Zhuang, Y.; Chen, D. Phenology-based classification of crop species and rotation types using fused MODIS and Landsat data: The comparison of a random-forest-based model and a decision-rule-based model. *Soil Tillage Res.* **2021**, *206*, 104838. [CrossRef]
47. Wang, H.; Magagi, R.; Goïta, K.; Trudel, M.; McNairn, H.; Powers, J. Crop phenology retrieval via polarimetric SAR decomposition and Random Forest algorithm. *Remote Sens. Environ.* **2019**, *231*, 111234. [CrossRef]
48. Du, P.; Samat, A.; Waske, B.; Liu, S.; Li, Z. Random Forest and Rotation Forest for fully polarized SAR image classification using polarimetric and spatial features. *ISPRS J. Photogram. Rem. Sens.* **2015**, *105*, 38–53. [CrossRef]
49. Story, M.; Congalton, R.G. Accuracy Assessment: A User's Perspective. *Photogramm. Eng. Remote Sens.* **1986**, *52*, 397–399.
50. Ifarraguerri, A.; Prairie, M.W. Visual Method for Spectral Band Selection. *IEEE Geosci. Remote Sens. Lett.* **2004**, *1*, 101–106. [CrossRef]
51. Chen, J.H.; Jia, W.X.; Zhao, Z. Research on temporal and spatial variation characteristics of vegetation cover of Qilian Mountains from 1982 to 2006. *Adv. Earth Sci.* **2015**, *30*, 834–845.
52. Meng, Z.J.; Rui, Z.Y.; Qin, J.M. Analysis on the importance of sample vegetation investigation in the continuous inventory of forest resources. *Inn. Mong. For. Investig. Des.* **2014**, *37*, 41–43. [CrossRef]

53. Tang, H.; Song, X.-P.; Zhao, F.A.; Strahler, A.H.; Schaaf, C.L.; Goetz, S.; Huang, C.; Hansen, M.C.; Dubayah, R. Definition and measurement of tree cover: A comparative analysis of field-, lidar- and landsat-based tree cover estimations in the Sierra national forests, USA. *Agric. For. Meteorol.* **2019**, *268*, 258–268. [CrossRef]
54. Punalekar, S.M.; Planque, C.; Lucas, R.M.; Evans, D.; Correia, V.; Owers, C.J.; Poslajko, P.; Bunting, P.; Chognard, S. National scale mapping of larch plantations for Wales using the Sentinel-2 data archive. *For. Ecol. Manag.* **2021**, *501*, 119679. [CrossRef]